

LOCAL MEASUREMENTS OF CURRENT DRIVE BY ELECTRON CYCLOTRON WAVES

*C.C. Petty, W.A. Cox¹, C.B. Forest², R.W. Harvey³, R.J. Jayakumar⁴,
L.L. Lao, Y.R. Lin-Liu⁵, J. Lohr, T.C. Luce, M.A. Makowski⁴,
P.A. Politzer, and R. Prater*

General Atomics, P.O. Box 85608, San Diego, California 92186-5608, USA.

¹State University of New York, Buffalo, New York, USA.

²University of Wisconsin, Madison, Wisconsin, USA.

³CompX, Del Mar, California, USA.

⁴Lawrence Livermore National Laboratory, Livermore, California, USA.

⁵National Dong Hua University, Shoufeng, Hualian, Taiwan

e-mail: petty@fusion.gat.com

Electron cyclotron current drive (ECCD) is a sensitive measure of the subtle balance between wave-induced diffusion and collisional relaxation in velocity space. Quantitative determination of the ECCD profile from internal magnetic measurements falls into three categories: deduction, induction, and modulation. The basis for these different analysis techniques is discussed in this paper, and examples are given from the DIII-D tokamak.

1. Introduction

The phenomenon of current drive is a sensitive measure of the interaction in velocity space between electrons and electron cyclotron (EC) waves [1]. Two separate velocity space effects are responsible for electron cyclotron current drive (ECCD). One effect, found by Fisch and Boozer [2], considers the selective heating of electrons traveling in one toroidal direction to decrease their collision frequency, and thus increase their contribution to the toroidal current compared to their unheated counterparts moving in the opposite direction. The other effect, found earlier by Ohkawa [3], drives current in the reverse direction when the heated electrons become mirror trapped in the toroidal geometry. Fokker-Planck codes contain a complete model of this wave-particle interaction, but experimental validation of the physics is needed. This is best accomplished by comparing a local measurement of the current density driven by EC waves to the theoretical computations.

Several methods are available for measuring the ECCD. The majority of studies on tokamaks and stellarators [4–6] have determined the magnitude of the ECCD using the 0-D circuit equation, which estimates the current drive from the difference in the surface loop voltage necessary to sustain the toroidal current with and without the EC power. This requires EC pulse lengths longer than the radial relaxation time of the loop voltage. This is a particularly accurate method in discharges with complete noninductive current drive, as recently achieved on TCV [7]; otherwise, the plasma resistivity needs to be known to subtract the ohmic current. However, the profile of the driven current cannot be determined accurately using only external magnetic measurements.

If internal magnetic measurements are available, then the location and width of the ECCD profile, in addition to the magnitude, can be measured even for small driven currents. In this case, EC pulse lengths shorter than the radial relaxation time of the loop voltage can be utilized because direct use is made of Faraday's law. Regardless of the specific analysis method, several quantities need to be known to experimentally determine a localized current drive source:

1. Internal magnetic field structure, *e.g.*, motional Stark effect (MSE), Zeeman splitting, or Faraday rotation measurements. This information is used to determine both the parallel current density (J_{\parallel}) as well as the parallel electric field (E_{\parallel}).
2. Electrical resistivity (η) if $E_{\parallel} \neq 0$. This is usually calculated from neoclassical theory using the measured plasma profiles.
3. Bootstrap current and other "background" noninductive current sources, such as neutral beam current drive (NBCD), unless a fiducial comparison is obtained (*e.g.*, co/counter comparison) or these currents are negligible.

This paper will focus on measuring the localized ECCD profile using MSE polarimetry data [8]. While MSE polarimetry measures the radial profile of the magnetic field pitch angle, this is essentially a measurement of the vertical magnetic field (B_z) since the toroidal magnetic field (B_{ϕ}) is well approximated by the vacuum toroidal magnetic field in tokamaks of conventional aspect ratio. Quantitative determination of the ECCD profile from the B_z profile falls into three categories: deduction, induction, and modulation, as discussed in the following sections.

2. Deductive Method

In the deductive approach, the noninductive current drive is found from the evolution of the poloidal magnetic flux per radian (ψ) obtained from a time series of magnetic equilibrium reconstructions [9]. The local B_z measurements from the MSE diagnostic are important for constraining the equilibrium reconstruction from a code such as EFIT [10] so that an accurate map of flux surface contours is obtained. The Grad-Shafranov equation specifies the toroidal current density as

$$J_{\phi} = RP'(\psi) + \frac{F(\psi)F'(\psi)}{\mu_0 R}, \quad (1)$$

where P is the plasma pressure, $F = RB_{\phi}$ is the poloidal current function, R is the plasma major radius, and z is the vertical position. Note that $B_z = (1/R) \partial\psi/\partial R$.

The deductive method, also called the loop voltage analysis method, uses Ohm's law to divide the reconstructed current density into its inductive and noninductive components. In general toroidal geometry, the current density and electric field are related by

$$\langle \vec{J}_{NI} \cdot \vec{B} \rangle = \langle \vec{J} \cdot \vec{B} \rangle - \frac{\langle \vec{E} \cdot \vec{B} \rangle}{\eta}, \quad (2)$$

where J_{NI} represents all sources of noninductive current drive (including the bootstrap current) and symbol $\langle \dots \rangle$ denotes the flux surface average. The parallel current density profile can be computed from Ampère's law by taking spatial derivatives of ψ . Using equilibrium reconstructions at several instances in time, the parallel electric field profile can be determined from Faraday's law [11],

$$\langle \vec{E} \cdot \vec{B} \rangle = F \left\langle \frac{1}{R^2} \right\rangle \left(- \frac{\partial \psi}{\partial t} \Big|_{\rho} - \frac{\rho^2 B_{\phi,0}}{q(\rho)} \rho_b \frac{d\rho_b}{dt} \right), \quad (3)$$

where $B_{\phi,0}$ is the vacuum field at the center of the vessel, q is the safety factor, and ρ is the normalized toroidal flux coordinate. The last term in Eq. (3) corrects for the time dependence of the effective minor radius of the plasma (ρ_b). The above equation is useful only in the absence of sawtooth relaxations and other strong MHD activity because these fluctuations complicate the electric field determination. Substituting Eq. (3) into Eq. (2) allows the parallel noninductive current density ($\langle J_{NI} \rangle \equiv \langle J_{NI} \cdot \vec{B} \rangle / B_{\phi,0}$) to be determined. To isolate the ECCD component, other sources of noninductive current drive like the bootstrap current and NBCD must be calculated and subtracted from $\langle J_{NI} \rangle$. Alternatively, a fiducial plasma with radial or counter-ECCD may be subtracted from a co-ECCD plasma to isolate the ECCD component more directly.

The deductive approach has been demonstrated to work well for distributed sources of noninductive current such as NBCD [9]. However, ECCD is a challenge for this method because the radial profile of the driven current may be very narrow, and it is difficult to reconstruct equilibria with this spatial resolution [12]. This limitation can be resolved by utilizing a basis set representation in EFIT that allows localized features with strong gradients in the current profile [13]. In particular, FF' can exhibit a large localized component due to ECCD, and can be fully described only if a local representation (such as a cosine square function) is added to the polynomial basis function. Figure 1 shows that equilibrium reconstructions using this local basis function can successfully resolve very peaked ECCD profiles in DIII-D. The variance in ψ from a linear evolution with time can be used to determine the experimental uncertainty in the parallel loop voltage ($V_{||} = 2\pi R_0 \langle E_{||} \rangle$). The experimental ECCD profile ($\langle J_{EC} \rangle$) in Fig. 1(c) is seen to agree with the theoretical ECCD profile calculated by the quasi-linear CQL3D Fokker-Planck code [14].

A recent variation of the deductive method solves the time derivative of the Grad-Shafranov equation and finds the profile of $\partial J_{\phi} / \partial t$ that best fits the experimental data [15]. The advantages of this approach are that a different basis set is allowed for the time dependent components of F' and P' , and offset errors in the experimental data are unimportant since only the time derivatives of the signals are used.

3. Inductive Method

In the inductive approach, the measured MSE signals are compared to simulations of the MSE evolution using a coupled transport-equilibrium code that contains a model for the location, width, and magnitude of the current drive source [12]. The parameters of the current drive model are varied systematically to minimize the difference between the measured and simulated MSE signals. This simulation approach is essentially the reverse of the loop voltage analysis method described in Sec. 2. Although the inductive method tends to be a brute force process, it has the advantage that the MSE signals are used directly, rather than being fitted as done by EFIT, so critical spatial information is not lost.

An accurate simulation of the magnetic equilibrium evolution is obviously the key element for using the inductive approach to interpret the MSE data during ECCD. Experiments in DIII-D have been analyzed using the

ONETWO code [16] that couples the 1-1/2 D transport calculations to a fixed boundary equilibrium code. The simulation uses the measured profiles (typically at 0.05 s intervals) of the electron density, electron and ion temperatures, toroidal rotation, and effective charge state. The transport code steps forward in time (typically by 0.01 s) and evolves the poloidal magnetic field and the parallel electric field using Faraday's and Ohm's laws, respectively, while the parallel current density is determined from Ampère's law. The poloidal current function is determined from the flux-surface-averaged toroidal current density and the experimental pressure profile, from which a new magnetic equilibrium is generated (again typically at 0.01 s intervals). The flux-surface-averaged NBCD and ECCD profiles, as well as the bootstrap current, are included in Ohm's law in the simulation. For convenience, the ECCD profile is modeled in this simulation using the TORAY-GA ray tracing code [17,18]. The parameters of the model — location, width, and magnitude — are adjusted until a best fit between the measured and simulated MSE signals is obtained.

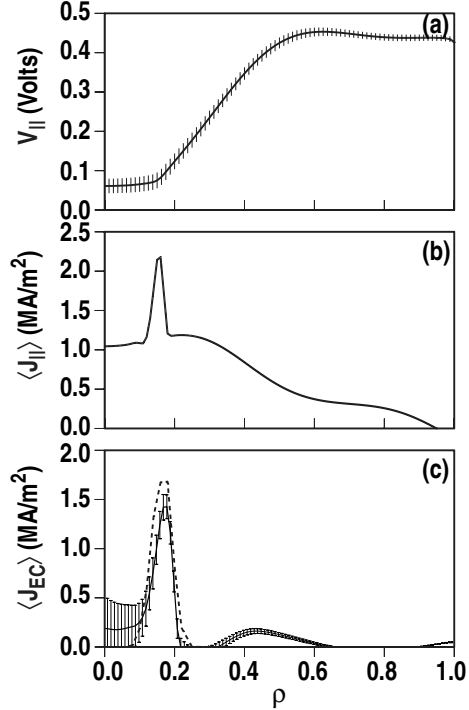


Fig. 1. Reconstructed profiles of (a) parallel loop voltage, (b) total parallel current density, and (c) parallel EC current density for DIII-D discharge 96163. The calculated ECCD profile using the CQL3D code (dashed curve) is also shown in (c).

Before using the simulated current evolution to infer the experimental ECCD, the predicted magnetic field pitch angles were benchmarked against the MSE data from plasmas with NBCD only. This is shown in Fig. 2 for a discharge without ECCD, where the value of the central safety factor was steadily decreasing from 2.2 to 1.0 over the plotted time interval. As with the deductive method, plasmas without sawteeth or other strong MHD activity are preferred for current drive analysis because the effect of these fluctuations on the current density evolution are not easily modeled. Figure 2 shows that the ONETWO code simulation agrees with the measured evolution of the magnetic field pitch angles provided that neoclassical resistivity is used.

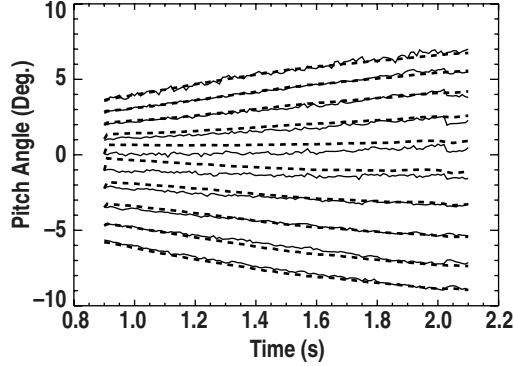


Fig. 2. Comparison of measured (solid curves) and simulated (dashed curves) evolution of the magnetic field pitch angles for DIII-D discharge 96161 without ECCD.

When comparing the measured and simulated MSE signals to determine the ECCD profile, it is convenient to convert the magnetic field pitch angles measured by MSE polarimetry to a quantity that is closely related to the local current density. Modeling the flux surfaces as concentric ellipses yields a relationship between the toroidal current density and vertical magnetic field that is accurate to within 10% for most plasma shapes of interest [19],

$$\mu_0 J_\phi = - \frac{B_z}{\kappa^2 (R - R_0)} - \frac{\partial B_z}{\partial R} \quad , \quad (4)$$

where R_0 is the major radius of the axis and κ is the plasma elongation. The solid lines in Fig. 3(a) show the measured change in the toroidal current density profile (ΔJ_ϕ) determined between a co-ECCD case in DIII-D and a similar discharge without ECCD. The figure shows that the ECCD is localized between two adjacent channels of the MSE system, or about 5 cm, on both sides of the magnetic axis located at $R_0 = 1.79$ m. This clearly illustrates the degree to which ECCD can be localized by the MSE diagnostic. The dashed lines in Fig. 3(a) show the simulated ΔJ_ϕ profile, which is in good agreement with the experimental points. The best fit ECCD profile, shown in Fig. 3(b), is in good agreement with the theoretical profile calculated using the CQL3D code.

4. Modulation Method

In the modulation approach, the ECCD profile is found directly from the periodic response of the MSE signals to a slow modulation of the EC power

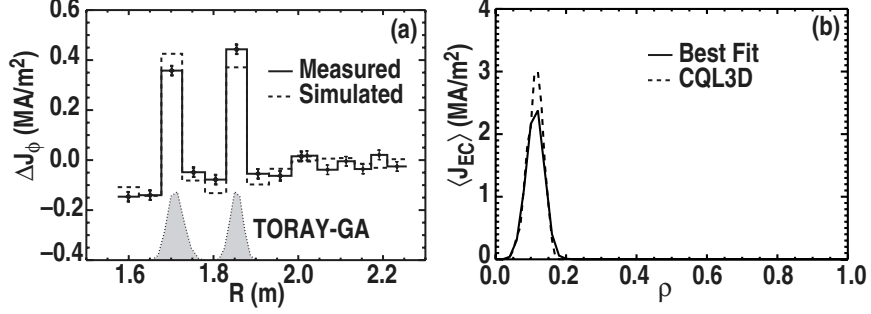


Fig. 3. (a) Change in the measured (solid lines) and simulated (dashed lines) toroidal current density as a function of major radius caused by co-ECCD for DIII-D discharge 104144. The magnetic axis is located at $R_0 = 1.79$ m and the ECCD profile calculated by the TORAY-GA code is indicated (not to scale). (b) Comparison of best fit ECCD profile from simulation (solid curve) to the predicted EC current density using the CQL3D code (dashed curve).

using the poloidal flux diffusion equation. This is analogous to measuring the EC power deposition profile by measuring the electron temperature (T_e) response to a fast modulation of the gyrotron power. The evolution of y is governed by a diffusion equation that is arrived at by combining the flux-surface-average Ohm's law and Maxwell's equations. In general toroidal geometry, this equation is

$$\left. \frac{\partial \psi}{\partial t} \right|_{\rho} - \rho \frac{\partial \psi}{\partial \rho} \frac{1}{\rho_b} \frac{d\rho_b}{dt} = \frac{\eta}{\mu_0 \rho_b^2 \hat{F}^2} \frac{1}{\rho} \frac{\partial}{\partial \rho} \left(\hat{F} \hat{G} \hat{H} \rho \frac{\partial \psi}{\partial \rho} \right) + \frac{R_0 \eta \hat{H}}{B_{\phi,0}} \left\langle \vec{J}_{NI} \cdot \vec{B} \right\rangle. \quad (5)$$

The three dimensionless geometry factors, defined as [16]

$$\hat{F} \equiv \frac{R_0 B_{\phi,0}}{F}, \quad \hat{G} \equiv \left\langle \frac{R_0^2}{R^2} \rho_b^2 |\vec{\nabla} \rho|^2 \right\rangle, \quad \hat{H} \equiv \frac{\hat{F}}{\sqrt{R_0^2/R^2}}, \quad (6)$$

tend towards unity in the infinite aspect ratio, low b , circular equilibrium limit. Considering for the moment the simplified situation where the plasma profiles, and flux surfaces do not oscillate, the Fourier transform of Eq. (5) yields an ordinary differential equation that relates the modulated ECCD source to the modulation in the poloidal magnetic flux,

$$\frac{\partial^2 \tilde{\psi}}{\partial \rho^2} + \left[\frac{1}{\rho} + \frac{\partial}{\partial \rho} \ln(\hat{F} \hat{G} \hat{H}) \right] \frac{\partial \tilde{\psi}}{\partial \rho} - \frac{i}{\hat{D}} \tilde{\psi} = -\mu_0 R_0 \rho_b^2 \frac{\hat{F}}{\hat{G}} \left\langle \tilde{J}_{EC} \right\rangle, \quad (7)$$

$$\hat{D} = \frac{\eta}{\mu_0 \rho_b^2 \omega} \frac{\hat{G} \hat{H}}{\hat{F}}, \quad (8)$$

where $\langle \tilde{J}_{EC} \rangle \equiv \langle \tilde{J}_{EC} \cdot \tilde{B} \rangle / B_{\phi,0}$. The mathematical form of Eq. (7) is analogous to that for heat pulse propagation (without the damping term), and the measured modulation in the MSE signals, $B_z = (1/R)\partial\tilde{\psi}/\partial R$, can be used to experimentally determine the modulated ECCD profile. The optimal modulation frequency is typically a few Hz owing to the small normalized diffusion coefficient (\tilde{D}). One useful feature of the modulation method is that fiducial comparison discharges are not needed to separate the modulated current drive from the unmodulated noninductive currents since the act of detrending the MSE data to remove the non-oscillating component serves this purpose.

There are several practical complications in using Eq. (7) to measure the ECCD profile. First, modulating all of the gyrotrons in phase will modulate η , as well as the bootstrap current (and NBCD if present), through a modulation of T_e . This may be avoided by using a “push/pull” setup where co- and counter-injecting gyrotrons at the same deposition location alternate during each cycle so that the total heating power remains constant with time. Second, if the plasma flux surfaces oscillate with the ECCD, then the right hand side of Eq. (7) becomes more complicated and is no longer simply proportional to the ECCD source. Fortunately, this appears to be a small effect. The final complication is that the MSE diagnostic actually measures B_z at fixed (R,z) coordinates rather than at a fixed ρ position. Therefore, the contribution of the electric field to the left hand side of Eq. (5) should be written as

$$\left. \frac{\partial\psi}{\partial t} \right|_{\rho} = \left. \frac{\partial\psi}{\partial t} \right|_{R,z} + \frac{\rho_b^2 B_{\phi,0}}{q} \rho \left. \frac{\partial\rho}{\partial t} \right|_{R,z} . \quad (9)$$

The last term in the above equation accounts for the oscillation in the mapping between ρ coordinates and (R,z) coordinates caused by the change in the magnetic topology related to the change in the plasma current profile. Unfortunately, this appears to be a significant effect except for very near the axis.

It is straightforward to solve the poloidal flux diffusion equation for the modulated ECCD source if the oscillating poloidal flux can be taken from measurements. The oscillating MSE signals can be Fourier analyzed and the resulting $B_z(R)$ profile integrated over major radius to convert it to $\tilde{\psi}$. The constant of integration can be taken from the measured oscillation in the surface loop voltage, but for most cases $V_{\phi,b} \approx 0$ because $\tilde{\psi}$ dissipates before reaching the plasma boundary. In the high frequency limit, which is usually approached since \tilde{D} is small except near the cold edge, the modulated ECCD profile is simply related to the oscillating MSE signals by

$$\langle \tilde{J}_{EC} \rangle = \frac{i\omega}{R_0\eta\tilde{H}} \tilde{\psi} = \frac{i\omega}{R_0\eta\tilde{H}} \left(- \int_{R_b}^R R\tilde{B}_z dR + \frac{i}{2\pi\omega} \tilde{V}_{\phi,b} \right) , \quad (10)$$

where R_b is the major radius of the plasma boundary on the low field side. The above equations show that while the $\tilde{\psi}$ mirrors the modulated ECCD profile, the MSE diagnostic actually records a null measurement ($B_z = 0$) at the peak location of the ECCD profile.

The expected MSE response to modulated off-axis ECCD, determined by numerically solving Eq. (7), is shown in Fig. 4 where the amplitude and phase of the fluctuating vertical magnetic field are plotted as a function of the major radius. The modulated ECCD source has a peak deposition around $\rho = 0.2$, which corresponds to $R = 1.59$ m on the plasma inboard midplane and $R = 1.92$ m on the plasma outboard midplane. The largest B_z occurs at locations that have a strong spatial gradient in the ECCD source; it should also be noted that the phase of B_z changes by 180 deg across the major radius of the ECCD peak. The plasma geometry factors and profiles of neoclassical resistivity and ECCD used in the numerical solution for B_z are taken from the DIII-D discharge shown in Fig. 5, which utilized alternating co/counter ECCD at 5 Hz as well as one neutral beam source to slow the current evolution and to continuously collect MSE data. Figure 5 shows that there is a small residual modulation of T_e because the co and counter heating powers were not matched. This caused a small undesired modulation in η that is neglected in the analysis presented here.

The measured MSE response to the modulated ECCD was in qualitative agreement with the numerical simulation, as shown in Fig. 4. A diminished amplitude for B_z was observed experimentally near the major radii of the predicted ECCD peak, and the expected 180 deg phase jumps near the peak

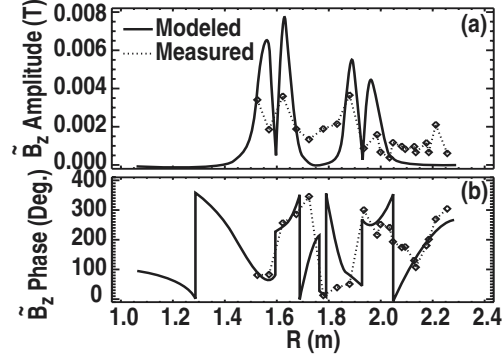


Fig. 4. (a) Amplitude and (b) phase (relative to EC power) of the oscillating vertical magnetic field measured by MSE polarimetry as a function of major radius during 5 Hz ECCD modulation for DIII-D discharge 115424. The modeled (solid curves) and measured (dotted curves & symbols) MSE responses are shown.

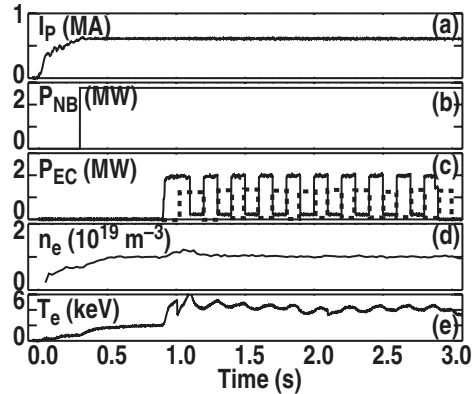


Fig. 5. Time history of DIII-D discharge 115424: (a) plasma current, (b) neutral beam power, (c) alternating co-ECCD (solid lines) and counter-ECCD (dashed lines) powers, (d) line average electron density, and (e) central electron temperature.

locations were also observed experimentally. Solving Eq. (7) for the oscillating current drive source gives the first direct measurement of the (flux-surface-average) ECCD profile using the modulation method, which is shown in Fig. 6. In this figure, only the component of $\langle J_{EC} \rangle$ that is in phase with the modulated EC power is plotted. A significant response was also observed that was 90 deg out of phase with the EC power; this is probably due to the undesired oscillations in the plasma shape and resistivity. Figure 6 shows that localized current drive was measured at the predicted ECCD location, and there was good overlap between the MSE points on the inboard and outboard sides of the axis. The magnitude of the ECCD profile was in approximate agreement with the TORAY-GA calculation.

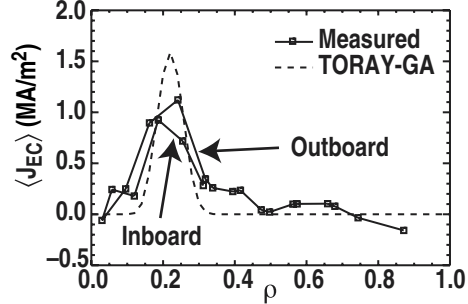


Fig. 6. Measured (solid curve & symbols) and theoretical (dashed curve) flux-surface-average ECCD profile for DIII-D discharge 115424.

Figure 6 shows that localized current drive was measured at the predicted ECCD location, and there was good overlap between the MSE points on the inboard and outboard sides of the axis. The magnitude of the ECCD profile was in approximate agreement with the TORAY-GA calculation.

5. Conclusions

The current density driven by EC waves is a sensitive probe of the wave-particle interaction in velocity space. There exist several different analysis techniques for determining the local ECCD profile from internal magnetic measurements such as those from MSE polarimetry. The deductive approach reconstructs the poloidal magnetic flux evolution from the MSE data, which allows the inductive and noninductive components of the current density to be separated. The inductive approach simulates the evolution of the MSE signals using a coupled transport-equilibrium code, and then adjusts the internal ECCD model to obtain a best fit with the measured MSE data. These two forms of current drive analysis are complementary with different strong and weak points. The loop voltage analysis method works robustly for current drive sources that are spatially extended, such as NBCD, while the MSE simulation method is well-suited to spatially localized current drive sources, such as off-axis ECCD. The biggest advantage of the MSE simulation approach is that the raw (or slightly manipulated) MSE signals are utilized, so critical spatial information is not lost to smoothing effects, while the biggest advantage for the loop voltage analysis method is that no assumptions need to be made about the profile of the current drive source. A third current drive analysis technique is to modulate the ECCD source and measure the resulting oscillation in the MSE signals. Fourier analysis of the poloidal flux diffusion equation shows that this yields a local measurement of the ECCD source in analogy to measuring the EC power deposition profile from the oscillations in T_e . It is encouraging that the first measured ECCD

profile using this new modulation technique was in agreement with the theoretically calculated profile.

Acknowledgment

Work supported by U.S. Department of Energy under DE-FC02-04ER54698, DE-FG03-99ER54541, DE-FG02-86ER53223, and W-7405-ENG-48. W.A. Cox was funded by the National Undergraduate Fellowships in Plasma Physics and Fusion Energy Sciences from the U.S. Department of Energy.

References

- [1] R. Prater, Phys. Plasmas **11**, 2349 (2004).
- [2] N.J. Fisch and A.H. Boozer, Phys. Rev. Lett. **45**, 720 (1980).
- [3] T. Ohkawa, "Steady State Operation of Tokamaks by r-f Heating," General Atomics Report GA-A13847 (1976).
- [4] V. Erckmann and U. Gasparino, Plasma Phys. Control. Fusion **36**, 1869 (1994).
- [5] B. Lloyd, Plasma Phys. Control. Fusion **40**, A119 (1998).
- [6] T.C. Luce, IEEE Trans. Plasma Sci. **30**, 734 (2002).
- [7] O. Sauter, *et al.*, Phys. Rev. Lett. **84**, 3322 (2000).
- [8] B.W. Rice, *et al.*, Phys. Rev. Lett. **79**, 2694 (1997).
- [9] C.B. Forest, *et al.*, Phys. Rev. Lett. **73**, 2444 (1994).
- [10] L.L. Lao, *et al.*, Nucl. Fusion **30**, 1035 (1990).
- [11] F.L. Hinton and R.D. Hazeltine, Rev. Mod. Phys. **48**, 239 (1976).
- [12] C.C. Petty, *et al.*, Nucl. Fusion **41**, (2001) 551.
- [13] L.L. Lao, *et al.*, in Radio Frequency Power in Plasmas (Proc. 14th Int. Conf. Oxnard, 2001), AIP, New York (2001) 310.
- [14] R.W. Harvey and M.G. McCoy, in Proceedings of the IAEA Technical Committee Meeting, Montreal, 1992 (IAEA, Vienna, 1993) p. 498.
- [15] J.K. Anderson, *et al.*, Phys. Plasmas **11**, L9 (2004).
- [16] H.E. St. John, *et al.*, in Plasma Physics and Controlled Nuclear Fusion Research (Proc. 15th Int. Conf. Seville, 1994), Vol. 3 (IAEA, Vienna, 1996) p. 603.
- [17] R.H. Cohen, Phys. Fluids **30**, 2442 (1987).
- [18] K. Matsuda, IEEE Trans. Plasma Sci. **17**, 6 (1989).
- [19] C.C. Petty, *et al.*, Nucl. Fusion **42**, 1124 (2002).